Negative exchange bias in single-phase Dy_{1−x}Nd_{x}CrO_{3} induced by Nd doping

A. McDannald, C. R. dela Cruz, M. S. Seehra, and M. Jain

Phys. Rev. B **93**, 184430 — Published 25 May 2016

DOI: 10.1103/PhysRevB.93.184430

Negative exchange bias in single phase $Dy_{1-x}Nd_xCrO_3$ induced by Nd doping

A. McDannald[1], C. R. dela Cruz[2], M. S. Seehra[3], and M. Jain[4,5]

[1]Materials Science and Engineering Department, University of Connecticut, Storrs, CT 06269
[2]Quantum Condensed Matter Division, Oak Ridge National Laboratory, Oak Ridge, TN 37831
[3]Department of Physics and Astronomy, West Virginia University, Morgantown, WV 26506
[4]Department of Physics, University of Connecticut, Storrs, CT 06269
[5]Institute of Material Science, University of Connecticut, Storrs, CT 06269

Abstract

Observation of significant negative exchange bias (H_E) is reported in solid-solutions of single phase samples of $Dy_{1-x}Nd_xCrO_3$ for x = 0.33, 0.67, and 1 with the corresponding Néel temperatures at T_N^{Cr} = 175 K, 200 K, and 225 K respectively, and the spin-reorientation transitions T_{SR} at 48 K, 58 K, and 38 K respectively. In contrast, no H_E was observed for the sample with x = 0 (i.e. $DyCrO_3$) shows no H_E below its T_N^{Cr} = 145 K and no reorientation of spins at lower temperatures was observed. More importantly, the (negative) H_E for the x = 0.33, 0.67, and 1 samples is observed only in the temperature range between T_N and T_{SR} with the corresponding observation of magnetic coercivity. These results show that the canted antiferromagnetic $\Gamma_{7,Cr}$ structure of the Cr^{3+} moments present between T_N^{Cr} and T_{SR} is essential for the observed H_E. By comparing this result to the literature, common features of single phase materials with H_E were identified. The present bulk powder samples were prepared by the citrate method and structurally characterized by x-ray diffraction and Raman spectroscopy techniques. Neutron diffraction measurements for the x = 0.33, 0.67, and 1 samples at select temperatures were done to verify the presence of the $\Gamma_{7,Cr}$ structure between T_N^{Cr} and T_{SR} and the $\Gamma_{1,Cr}$ structure (with no canting of Cr^{3+} moments) below T_{SR}.

I. INTRODUCTION

Magnetic exchange bias (H_E) refers to the observation of a shifted and an asymmetric hysteresis loop in a multiphase magnetic material involving different phases such as a ferromagnet (FM), ferrimagnet (FIM), antiferromagnetic (AFM), and/or a spin glass. This H_E phenomenon is understood to result from unidirectional anisotropy induced in the FM component by the AFM component. Exchange coupling at the interface between the two different magnetic phases causes the anisotropy in the FM component when the sample is cooled through the Néel temperature (T_N) of the AFM material in a magnetic field.[1] In recent years, the H_E phenomenon has acquired enormous technological importance because of its utilization in modern spin-valve devices, magnetic recording devices, thermally assisted random access memory, and spintronic devices.[1–7] In addition to layers of a FM material on a AFM material, the H_E effect has also been observed in core-shell geometries.[8]

There are a few accepted theoretical descriptions of H_E that include more influences than the simple exchange coupling at a FM/AFM interface developed by Meiklejohn and Bean.[9,10] For example, the in the Domain State model, the ease of domain formation in the bulk of a diluted AFM contributes to the interface magnetization and therefore H_E.[11,12] The accepted theoretical descriptions of H_E have been developed for systems that satisfy two conditions. First, the FM and AFM materials are spatially distinct, which allows for the uncompensated spins (or distortion of the AFM ordering) at the interface. Second, the Curie temperature (T_C) of the FM phase is higher than the T_N of the AFM phase. This allows for the FM to influence the AFM ordering pattern (*i.e.* the direction of the first layer of spins in the AFM with respect to the FM) as the AFM is cooled below T_N. The now frozen AFM ordering below T_N establishes a preferential orientation of the FM, which manifests as the H_E.

Yet, there have been a few recent reports of H_E in bulk single phase materials which satisfy neither of the above conditions for the theoretical descriptions of exchange bias. In these systems, the presence of the exchange bias has been attributed to different mechanisms. For example, in the double perovskite Sr_2YbRuO_6 the H_E was thought to arise from the competition between the Dzyaloshinskii-Moriya interaction (DMI) and uniaxial anisotropy.[13] In $NdCr_{1-x}Fe_xCrO_3$, the observed H_E was explained by the exchange anisotropy between the canted Cr^{3+} moments and the Nd^{3+} and Fe^{3+} moments.[14] Mao *et al.* claimed that the competition between DMI and single-ion anisotropy is responsible for the observed H_E in $YCr_{0.5}Fe_{0.5}O_3$.[15] Short range magnetic order in the rare-earth sublattice of $NdMnO_3$ was presented as a basis for the observed H_E in that material.[16] Although the theories describing the cause of the H_E differ widely, there are common features in the reports of the magnetic properties of the aforementioned material systems. All of these systems are primarily AFM with a canting that results in weak FM behavior. Additionally, all of these material systems contain more than one magnetic ion, typically separated into different sublattices. Furthermore, magnetic reversal is observed in all of the aforementioned materials under field cooled conditions.

The rare-earth chromites ($RCrO_3$) are canted AFM materials with multiple magnetic ions. Rare-earth ion, Dy^{3+} has the highest effective magnetic moment of all the trivalent rare-earth ions and in $DyCrO_3$, the moment of Dy^{3+} is thought to co-align along the canted moment of the Cr^{3+} sublattice.[17] The $NdCrO_3$ does not exhibit magnetic reversal, but the moment of Nd^{3+} is thought to oppose the canted moment of the Cr^{3+} sublattice.[17] These materials stabilize in an orthorhombically distorted perovskite structure with a *Pnma* (alternatively *Pbnm*) space group.[18] The Cr^{3+} ions are at the octahedrally coordinated B-sites, while the R^{3+} ions are at the 12-fold coordinated A-sites. The chromium sublattice orders as a G-type antiferromagnet at temperatures between 110 K and 220 K depending on the rare-earth ion.[17] The different possible arrangements of this magnetic order will be discussed in more detail in the following sections. The rare-earth ion typically orders at much lower temperatures (< ~10 K). The $RCrO_3$ materials are additionally interesting due to their magnetic properties and potential as magnetoelectric multiferroics.[19,20] The solid-solution of $NdCrO_3$ ($T_N \approx 210$ K) and DCO ($T_N \approx 146$ K) is therefore also interesting as a means of shifting the T_N higher, toward application relevant operating conditions.

In this study, the structural and magnetic properties of $Dy_{1-x}Nd_xCrO_3$ solid-solutions were studied. An exchange bias was observed in these samples that varies as the Dy^{3+} ions are substituted for the Nd^{3+} ions. Our results show that exchange bias in a single phase material can be observed without a magnetic reversal.

II. EXPERIMENTAL

Powder samples of the four compositions of $Dy_{1-x}Nd_xCrO_3$ for x =0, 0.33, 0.67, and 1 were synthesized by a citrate method. In this procedure, stoichiometric amounts of nitrates of Dy, Nd, and Cr were dissolved in water at 70°C before the addition of citric acid. The resultant solutions were dried on a hot plate and subsequently annealed at 900°C for 2 hours in an O_2 atmosphere. X-ray diffraction (XRD) measurements of the annealed powders were performed on a Bruker D5 diffractometer using Cu-Kα radiation. Raman spectra were recorded at room temperature using a 514 nm Argon laser in the Renishaw System 2000. Magnetic characterization was done using a vibrating sample magnetometer option attached to an Evercool Physical Property Measurement System (from Quantum Design). Neutron diffraction experiments were carried out at the HB-2A high resolution neutron powder diffractometer at the High Flux Isotope Reactor at the Oak Ridge National Laboratory using the wavelength λ=2.4067 Å. The collimation of the HB-2A beamline used was open-21'-12', pre-monochromator, pre-sample and pre-detector, respectively. The FullProf Suite software package was used for Rietveld refinement of the neutron diffraction data.[21]

III. STRUCTURAL CHARACTERIZATION

A. X-ray diffraction:

Powder XRD measurements (Figure 1) were performed in order to determine the phase purity of the prepared $Dy_{1-x}Nd_xCrO_3$ samples (x =0, 0.33, 0.67, and 1). All the observed diffraction peaks belonged to the aforementioned *Pnma,* an orthorhombically distorted perovskite structure. A systematic shift in the position of the diffraction peaks as a function of x, from $DyCrO_3$ to $NdCrO_3$, was observed. The lattice parameters, as determined from the diffraction patterns, also show a systematic trend (see Figure 2). With increasing x, the out-of-plane 'b' and in-plane 'c' lattice parameters as well as the unit cell volume (V) (see inset of Figure 2) increase, while the in-plane 'a' lattice parameter decreases. The lattice parameters of the present samples with x = 0 and 1 agree well with those reported by Weber *et al.* for $DyCrO_3$ and $NdCrO_3$, respectively.[18] The monotonic increase in V with increasing x is expected since the ionic radius of Nd^{3+} is larger than that of Dy^{3+}.[22] According to the Rietveld refinement of the diffraction patterns the lattice parameters have uncertainties less than 0.016 Å. These results suggest that the present synthesis method resulted in a single phase materials of solid-solution $Dy_{1-x}Nd_xCrO_3$.

B. Raman Spectroscopy:

Raman spectra were measured at room temperature (Figure 3) to compliment the structural characterization by XRD. The structure of $RCrO_3$ is known to have 24 Raman active modes, 12 of which occur in the range of 100 cm^{-1} to 600 cm^{-1}.[18] The positions of the Raman modes of the present samples also show a systematic variation with x. For example, the Raman peak at ~488 cm^{-1} for x = 0 (the superposition of the B_{3g} out-of-phase O2 scissor-like phonons, an A_g mode from CrO_6 bending, and a B_{2g} mode from CrO_6 out-of-phase bending) show a smooth transition to the asymmetric peak at ~447 cm^{-1} seen for x = 1. This result is consistent with the findings of Weber *et al.* who showed a systematic shift in the positions of these modes toward lower wave numbers with increasing A-site atomic radius.[18] The CrO_6 rotations are the main distortions from the ideal cubic structure, and therefore a shift toward lower wave numbers of those phonon modes is expected as the A-site radius approaches that of the ideal perovskite. With increasing A-site ionic radius, the modes between 400 cm^{-1} and 200 cm^{-1} also shift toward the lower wave numbers, while the modes below 200 cm^{-1} shift toward higher wave numbers.[18] The combined effect in the shift of these phonon modes is that the peaks in the Raman spectra become less distinct with larger A-site radius, as observed in the present spectra of the samples studied here. Because both XRD scans and Raman spectra show a systematic shift in the positions of the observed peaks without noticeable broadening, it is clear that the synthesis method was successful in substituting Nd for Dy in $DyCrO_3$ without noticeable phase separation or impurity phases. If phase separation was present, a peak splitting (due to the superposition of the Dy-rich and Nd-rich responses) would be expected.[23] However, such splitting was not observed indicating that the present samples are likely phase pure.

C. Neutron Diffraction:

In order to determine the influence of the Nd substitution on the magnetic structure of $DyCrO_3$, neutron diffraction measurements of $Dy_{1-x}Nd_xCrO_3$ powder samples with $x = 0.33$ and 0.67 were performed at the select temperatures. The magnetic structures of the end compounds are well known and have been summarized by Hornreich.[17] The Cr^{3+} sublattice of $DyCrO_3$ forms in the irreducible representation $\Gamma_{7,Cr}$ structure, which is a G-type AFM along the *b*-axis with a slight ferromagnetic canting along the *c*-axis. In $NdCrO_3$, the Cr^{3+} sublattice also forms in the $\Gamma_{7,Cr}$ structure, but undergoes a spin-reorientation at 33 K to a $\Gamma_{1,Cr}$ structure, which is a G-type AFM along the *a*-axis with no canting.

The magnetic structures of the present samples were measured at several different temperatures using a 2.4067 Å wavelength neutron beam. Representational analysis, done using SARA*h*,[24] was employed on both the Cr^{3+} and R^{3+} sublattices in order to determine the symmetry compatible magnetic structures at low temperatures. Refinement models using single irreducible representations (irreps) were built using the allowed irreps ($\Gamma_{1,Cr}$, $\Gamma_{3,Cr}$, $\Gamma_{5,Cr}$, or $\Gamma_{7,Cr}$ for the Cr^{3+} sublattice, and $\Gamma_{1,Nd}$, $\Gamma_{2,Nd}$, $\Gamma_{3,Nd}$, $\Gamma_{4,Nd}$, $\Gamma_{5,Nd}$, $\Gamma_{6,Nd}$, $\Gamma_{7,Nd}$, or $\Gamma_{8,Nd}$ for the R^{3+} sublattice) consistent with the magnetic propagation vector $\mathbf{k} = (0,0,0)$ in the *Pnma* nuclear space group. The fitting was attempted with each of the Cr^{3+} irreducible representations and the structure was determined by comparing the quality of the fittings. At lower temperatures, where a single irrep of the Cr^{3+} structure was insufficient to describe the observed diffraction pattern, combinations with other irreps as well as combinations with the irreps of the R^{3+} structure were also considered. The aluminum from the sample holder was also included in the refinement as a separate phase.

As will be discussed in greater detail in a later section, a magnetic H_E was observed under field-cooled conditions for the samples with $x = 0.33$, 0.67, and 1. Therefore, neutron diffraction measurements were also performed under field cooled conditions for the powder samples with $x = 0.67$ and 1. In order to perform these measurements, the bulk powder samples were pressed and sintered into pellet form to prevent rotation of domains under the influence of an applied magnetic field. The pellets were contained in vanadium sample holders. The neutron diffraction experiments were performed at several temperatures under both zero-field cooled (ZFC) and 2 T field cooled (FC) conditions. Figure 4 shows Rietveld refinements for $x = 0.67$ at several temperatures under ZFC conditions. For all x as the samples were cooled, the $\Gamma_{7,Cr}$ structure of the Cr^{3+} sublattice was the first magnetically ordered phase observed. In this magnetic structure the Cr^{3+} spins are ordered in G-type AFM structure, with the moments along the *b*-axis and a slight canting toward the *a*-axis. Upon further cooling, the samples with $x = 0.33$, 0.67, and 1 undergo a spin-reorientation to $\Gamma_{1,Cr}$. The $\Gamma_{1,Cr}$ is the Cr^{3+} spins in a G-type AFM structure with the moments along the *a*-axis, and a C-type AFM component along the *b*-axis. Pure $NdCrO_3$ also shows magnetic ordering of the Nd^{3+} moments in the $\Gamma_{7,Nd}$ structure below 10 K. This $\Gamma_{7,Nd}$ structure is the Nd^{3+} spins in an A-type AFM structure with the moments along the *a*-axis. Under 2 T field cooling conditions, this R^{3+} ordering is also observed in the sample with $x = 0.67$. Note that for ZFC conditions where $x = 1$ and $T \leq 10$ K and for FC conditions where $x = 0.67$, and 1 and $T \leq 10$ K, linear combinations of irreps of the Cr^{3+} did not fit the data well. Additionally, while linear combinations of $\Gamma_{1,Cr}$ and $\Gamma_{7,Nd}$ fit the data best under these conditions, the

differences between the quality of the fittings for $\Gamma_{1,Cr}$, combined with $\Gamma_{3,Nd}$, $\Gamma_{5,Nd}$, or $\Gamma_{7,Nd}$ were slight.

IV. RESULTS FROM MAGNETIC MEASUREMENTS

The magnetic transition temperatures can be resolved by ZFC and FC magnetization measurements, which were taken using a 50 Oe magnetic field for this study. The $\Gamma_{7,Cr}$ structure is expected to exhibit a large effective moment and hence bulk magnetization due to the ferromagnetic canting. On the other hand the $\Gamma_{1,Cr}$ structure, being purely AFM for the Cr^{3+} sublattice and paramagnetic in the R^{3+} sublattice, should have a much weaker moment and smaller bulk magnetization. As can be seen in Figure 5, the Néel temperature (T_N^{Cr}) of the present samples systematically increases with increasing *x*. Also, it is noted that the magnitude of the magnetization systematically decreases with increasing *x*. This is to be expected since Dy^{3+} has a much higher theoretical effective magnetic moment (μ_{eff} =10.65 μ_B) than Nd^{3+} (μ_{eff} =3.62 μ_B). The spin-reorientation transition from $\Gamma_{7,Cr}$ to $\Gamma_{1,Cr}$ is also evident in each of the present samples containing Nd^{3+}, manifesting as a peak in the FC data. The spin-reorientation transition (T_{SR}) was observed at 47.5 K, 57.5 K, 37.5 K for x = 0.33, 0.67, and 1, respectively. Another important feature in the x = 1 FC data is the decrease in effective magnetic moment between 175 K and 100 K, as shown in the inset of Figure 5d. This suggests that the Nd^{3+} and Cr^{3+} moment orientation in their sublattices are opposed. However, the Nd^{3+} sublattice is not strong enough to fully compensate the effective Cr^{3+} sublattice moment. In the x = 0.33 and 0.67 samples the anti-alignment of Nd^{3+} and Cr^{3+} could be masked by the behavior of the much stronger Dy^{3+} moments. Similar antialignment has been observed in single phase systems that show H_E. For example in Sr_2YbRuO_6, and $NdCr_{1-x}Fe_xO_3$ a magnetic reversal is observed upon field cooling due to the anti-alignment of the rare-earth and transition metal sublattices.[13,14]

In order to further understand the magnetic behavior of samples in the $Dy_{1-x}Nd_xCrO_3$ solid-solution, isothermal magnetization measurements were performed for each of the present samples at 100 K (Figure 6). As noted in our previous work on $DyCrO_3$, the measured magnetization can be approximately described as the superposition of a linear contribution and ferromagnetic contribution.[25] The linear component, which can clearly be seen in Figure 6a-d, is thought to comprise of the paramagnetic rare-earth sublattice as well as the pure AFM contribution from the Cr^{3+} sublattice.[26] The ferromagnetic contribution is due to the canting of the Cr^{3+} moments, and is most likely influenced by any asymmetric R-Cr exchange interactions, as has been reported for other similar rare-earth chromites.[26] Although difficult to see in Figure 6, the magnetic hysteresis loops close at 12 kOe, 30 kOe, and 28 kOe for x = 0, 0.33, and 0.67, respectively. For x = 1, there is no significant coercive field at 100 K. It can be seen in Figure 6a-d that at 100 K the coercive field, H_C, systematically decreases with increasing *x*. A negative H_E, in each of the x = 0.33, 0.67, and 1 samples can also be observed in Figure 6e-h. This H_E is shown to systematically increase with increasing *x*. In $NdMnO_3$ a negative H_E has been reported at low cooling fields at 30 K.[16] Hong *et al*. show that this H_E in $NdMnO_3$ becomes positive with

cooling fields of 8 T or greater. Additionally, the H_E in $NdMnO_3$ becomes positive at 8 K, which is below the compensation temperature in that material.[16] Figure 7 shows H_C and H_E measured under various field cooled conditions up to 90 kOe for the present x = 0.67 sample, which is representative of the behavior observed in the x = 0.33 and 1 samples. The H_C is unaffected by the strength of the cooling field. The H_E, however, is shown to quickly saturate with cooling field strength, reaching 92% of the -1455 Oe saturated H_E with a cooling field of only 500 Oe. Similar quick saturation of H_E was also observed in the x = 0.33 and 1 samples. Unlike $NdMnO_3$, H_E of the present samples does not become positive for cooling fields up to 90 kOe. The temperature dependences of H_C and H_E as extracted from successive isothermal magnetization measurements, are plotted in Figure 8 for the present samples. The largest H_E = -2212 Oe is observed for x = 1 at 170 K, and becomes smaller with decreasing x.

By combining the results of both the neutron diffraction measurements and the magnetic measurements, phase diagrams for the $Dy_{1-x}Nd_xCrO_3$ solid-solution are proposed under both ZFC (Figure 9) and FC (Figure 10) conditions. The T_N^{Cr} and the T_{SR} (as determined from the measurements of temperature dependence of the susceptibility) are also shown as the boundaries between the paramagnetic, $\Gamma_{7,Cr}$, and $\Gamma_{1,Cr}$ phases in the phase diagrams in Figures 9 and 10. The blue arrows in these diagrams represent the Cr^{3+} spins. In the $\Gamma_{7,Cr}$ structure the G-type AFM arrangement with the moments along the *b*-axis can be seen, as well as the canting toward the *c*-axis. The $\Gamma_{1,Cr}$ structure is shown in two of the diagrams. This is a G-type AFM structure with the moments along the *a*-axis. At low temperatures (in the region of the phase diagram highlighted in magenta), the $\Gamma_{1,Cr}$ structure also includes a C-type AFM component along the *b*-axis. This region additionally has the ordered Nd^{3+} moments, represented as green arrows in the diagrams. This $\Gamma_{7,Nd}$ structure is an A-type AFM arrangement with the moments along the *a*-axis. The increase size of the $\Gamma_{7,Nd}$ phase in both the ZFC and FC phase diagrams are consistent with the neutron diffraction results at 10 K and 1.8 K for x = 0.67, and 10 K and 1.6 K for x = 1. Note that the exchange bias is only observed in the $\Gamma_{7,Cr}$ phase (between the paramagnetic and $\Gamma_{1,Cr}$ phases) under FC conditions. This region has been highlighted in the FC phase diagram (Figure 10).

V. DISCUSSION

In all of the samples investigated here containing Nd^{3+}, peaks in the coercive field are observed at the T_N^{Cr} and T_{SR}, becoming more pronounced with increasing Nd content (Figure 8). The peaks in the coercive field correspond to the onset and subsequent disappearance of the H_E. This clearly shows that, in correlation to the neutron measurements, the H_E in each of the present samples only occurs in the $\Gamma_{7,Cr}$ phase, in which the Cr^{3+} moments are canted from the pure G-type AFM resulting to an effective ferromagnetic component. The H_E is not observed in the $\Gamma_{1,Cr}$ phase, which is not canted. $DyCrO_3$ (x = 0), also forms in the $\Gamma_{7,Cr}$ phase, however, no H_E is observed. Note that, unlike Nd^{3+}, the Dy^{3+} moments are thought to co-align with that of Cr^{3+}, which is consistent with the FC behavior shown in Figure 5a. Recall from the aforementioned neutron diffraction results that only a single irreducible representation was needed to model the

magnetic diffraction data at each temperature. Therefore, the accepted models of H_E, which necessitates a spatial distinction between FM and AFM materials, may not explain the exchange bias in the present system. In the Meiklejohn and Bean model, the uncompensated spins of the AFM at the interface with a FM cause the exchange bias.[9] Both the Mauri as well as the Kim & Stamps models rely on domain wall physics between a FM and AFM to allow for exchange bias with a fully compensated AFM interfacial layer.[27] However, none of the above theories can account for H_E observed in the interpenetrating sublattices of the present $Dy_{1-x}Nd_xCrO_3$ samples. Furthermore, the above models for H_E require that the T_C of the FM is higher than the T_N of the AFM.[27] This allows for the FM phase to influence the AFM ordering as the system is field cooled below T_N. However, in the present samples, in the 30 K to 215 K temperature range in which exchange bias is observed, only the Cr^{3+} sublattice is ordered. The net magnetic moment observed in the $\Gamma_{7,Cr}$ results from the canting of the Cr^{3+} spins in the G-type AFM structure, but there is only one magnetic phase. The Domain State model accounts for domain formation in a diluted AFM, which modifies the magnetization at the FM/AFM interface.[11,12] In this model, defects in the bulk of the AFM material can cause domain formation that leads to net magnetization at the FM/AFM interface. This model could be extended to systems of mixed FM and AFM materials, and possibly to continuous systems where the AFM component imposes a net field on the FM (as in case of a canted AFM sublattice and a FM sublattice). However, this model would need to be developed further to explain (i) why the H_E would be observed in $NdCrO_3$ and not in $DyCrO_3$ and (ii) why this H_E is observed when only the Cr^{3+} sublattice is ordered. Therefore, the above models are insufficient to describe the H_E observed in the present $Dy_{1-x}Nd_xCrO_3$ system, and new models must be developed. The fact that the onset of the exchange bias corresponds with the reduction of the coercive field suggests that the same mechanism that controls the exchange bias must also affect the coercive field. For $x = 0$, the competition between these two mechanisms, which are dominated by the R-Cr interaction, favors larger coercive fields and transitions to favor exchange bias as the value of x in $Dy_{1-x}Nd_xCrO_3$ increases toward 1.

Combining the results reported in this work as well as that from published literature, there are three common features of the materials in which an H_E is observed in a single phase: (1) there are more than one magnetic sublattice (i.e. transition metal and rare-earth, or two transition metals), (2) one magnetic sublattice forms in a canted AFM structure, and (3) the magnetic sublattices tend to counter align. These conditions are not only satisfied by the present samples (x = 0.33, 0.67, and 1), but are also valid for other reports of H_E in single phase materials including: $La_{1-x}Pr_xCrO_3$,[28] $NdCr_{1-x}Fe_xO_3$,[14] Sr_2YbRuO_6,[13] $YFe_{0.5}Cr_{0.5}O_3$,[15] and $NdMnO_3$.[16] The success of these conditions warrants further investigation into other materials, such as $TbMn_{0.3}Cr_{0.7}O_3$,[29] where H_E in single phase might be observed. The DMI within the magnetic sublattice is usually responsible for the canting of the AFM ordering, as is the case with the Cr^{3+} sublattice in $DyCrO_3$.[26] There are also suggestions that the DMI is responsible for the H_E in single phase systems,[14,15] however such a mechanism fails to explain why H_E would not be observed in $DyCrO_3$ in the present case. Another common proposed mechanism for H_E is

core-shell interaction, as in nanoparticles of Co_3O_4.[30] This mechanism does not seem to be active here since the present particles are bulk powders, not nanosized, and this also fails to explain the absence of H_E in $DyCrO_3$. Hong et al. suggest that, for $NdMnO_3$, the H_E is caused by local order of the Nd^{3+} moments which are antiferromagnetically coupled to the Mn^{3+} sublattice.[16] However, the present neutron diffraction experiments show no evidence of local order. Furthermore, the H_E in the present samples is only observed in the higher temperature $\Gamma_{7,Cr}$ phase, well above the Nd^{3+} ordering temperature. Clearly, a new mechanism for H_E is needed that considers the common features of multiple anti-coupled magnetic sublattices where one of magnetic structures is a canted AFM.

VI. CONCLUSIONS

In this work, samples of $Dy_{1-x}Nd_xCrO_3$, for x = 0, 0.33, 0.67, and 1, were synthesized by a citrate method. Analysis of x-ray diffraction and Raman spectroscopy measurements showed that the samples were phase pure. Neutron diffraction was performed for the x = 0.33, 0.67, and 1 samples in ZFC and FC conditions, from which magnetic phase diagrams are proposed. From the temperature dependence of the magnetization, a systematic increase in the Néel temperature with increasing x is reported. An observed decrease in the field cooled magnetization upon cooling in the x = 1 sample confirmed the tendency of the Nd^{3+} sublattice to oppose that of the Cr^{3+} sublattice. An exchange bias was observed in the x = 0.33, 0.67, and 1 samples, which quickly saturates with the strength of the cooling field. The temperature dependence of the coercive field and the exchange bias revealed that the exchange bias is only present in the canted antiferromagnetic $\Gamma_{7,Cr}$ phase. From these results, it is observed that there are three features of the magnetic structure that the present results have in common with other reports of exchange bias in a single material: (1) there are at least two magnetic sublattices, (2) one of the sublattices is a canted antiferromagnet, (3) the sublattices are anti-coupled. These conditions are met not only in the present samples (for x = 0.33, 0.67, and 1), but also in reports of exchange bias in wide array of other single phase materials.[13–16,28]

Acknowledgements:

This paper is based in part upon the work supported by the National Science Foundation Grant DMR No. 1310149. Research conducted at ORNL's High Flux Isotope Reactor was sponsored by the Scientific User Facilities Division, Office of Basic Energy Sciences, U.S. Department of Energy.

References:

[1] J. Nogués and I.K. Schuller, J. Magn. Magn. Mater. **192**, 203 (1999).

[2] C. Chappert, A. Fert, and F.N. Van Dau, Nat. Mater. **6**, 813 (2007).

[3] X. Chen, A. Hochstrat, P. Borisov, and W. Kleemann, Appl. Phys. Lett. **89**, 202508 (2006).

[4] V. Laukhin, V. Skumryev, X. Martí, D. Hrabovsky, F. Sánchez, M. García-Cuenca, C. Ferrater, M. Varela, U. Lüders, J. Bobo, and J. Fontcuberta, Phys. Rev. Lett. **97**, 227201 (2006).

[5] C. Binek and B. Doudin, J. Phys. Condens. Matter **17**, L39 (2005).

[6] T. Zhao, A. Scholl, F. Zavaliche, K. Lee, M. Barry, A. Doran, M.P. Cruz, Y.H. Chu, C. Ederer, N. A. Spaldin, R.R. Das, D.M. Kim, S.H. Baek, C.B. Eom, and R. Ramesh, Nat. Mater. **5**, 823 (2006).

[7] L.W. Martin and R. Ramesh, Acta Mater. **60**, 2449 (2012).

[8] V. Skumryev, S. Stoyanov, Y. Zhang, G. Hadjipanayis, D. Givord, and J. Nogués, Nature **423**, 850 (2003).

[9] W. Meiklejohn and C. Bean, Phys. Rev. **105**, 904 (1957).

[10] M. Kiwi, J. Magn. Magn. Mater. **234**, 584 (2001).

[11] U. Nowak, K.D. Usadel, J. Keller, P. Miltényi, B. Beschoten, and G. Güntherodt, Phys. Rev. B **66**, 014430 (2002).

[12] U. Nowak, A. Misra, and K.D. Usadel, J. Appl. Phys. **89**, 7269 (2001).

[13] R.P. Singh, C. V. Tomy, and A.K. Grover, Appl. Phys. Lett. **97**, 182505 (2010).

[14] T. Bora and S. Ravi, J. Magn. Magn. Mater. **386**, 85 (2015).

[15] J. Mao, Y. Sui, X. Zhang, Y. Su, X. Wang, Z. Liu, Y. Wang, R. Zhu, Y. Wang, W. Liu, and J. Tang, Appl. Phys. Lett. **98**, 192510 (2011).

[16] F. Hong, Z. Cheng, J. Wang, X. Wang, and S. Dou, Appl. Phys. Lett. **101**, 102411 (2012).

[17] R. Hornreich, J. Magn. Magn. Mater. **7**, 280 (1978).

[18] M.C. Weber, J. Kreisel, P.A. Thomas, M. Newton, K. Sardar, and R.I. Walton, Phys. Rev. B **85**, 054303 (2012).

[19] B. Rajeswaran, D.I. Khomskii, A.K. Zvezdin, C.N.R. Rao, and A. Sundaresan, Phys. Rev. B **86**, 214409 (2012).

[20] A. Ghosh, A. Pal, K. Dey, S. Majumdar, and S. Giri, J. Mater. Chem. C (2015).

[21] J. Rodríguez-Carvajal, T. Roisnel, J. Gonzalez-Platas, and L.C. Chapon, (2011).

[22] R.D. Shannon, Acta Crystallogr. Sect. A **32**, 751 (1976).

[23] T. Pichler, M. Matus, J. Kürti, and H. Kuzmany, Phys. Rev. B **45**, 13841 (1992).

[24] A.S. Wills, Phys. B Condens. Matter **276-278**, 680 (2000).

[25] A. McDannald, L. Kuna, and M. Jain, J. Appl. Phys. **114**, 113904 (2013).

[26] A. McDannald, L. Kuna, M.S. Seehra, and M. Jain, Phys. Rev. B **91**, 224415 (2015).

[27] F. Radu and H. Zabel, *Magnetic Heterostructures* (Springer Berlin Heidelberg, Berlin, Heidelberg, 2008).

[28] K. Yoshii, Appl. Phys. Lett. **99**, 142501 (2011).

[29] M. Staruch and M. Jain, J. Phys. Condens. Matter **26**, 046005 (2014).

[30] P. Dutta, M.S. Seehra, S. Thota, and J. Kumar, J. Phys. Condens. Matter **20**, 015218 (2008).

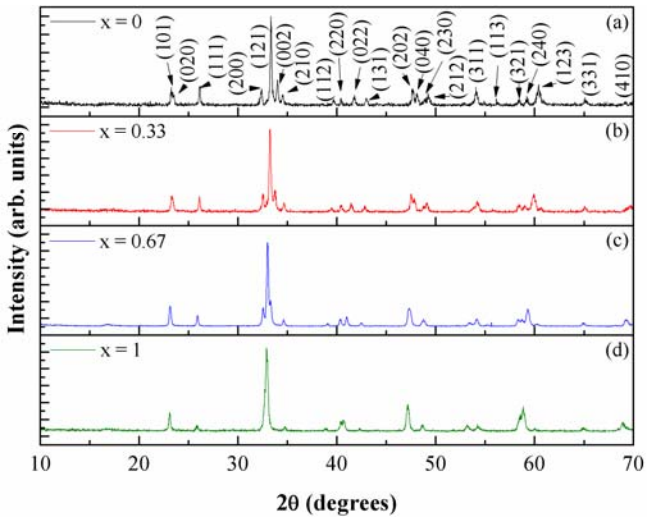

Figure 1: X-ray diffraction patterns of $Dy_{1-x}Nd_xCrO_3$ for x = 0, 0.33, 0.67, and 1 (a-d) showing that the materials synthesized in the *Pnma* phase with no observable impurities.

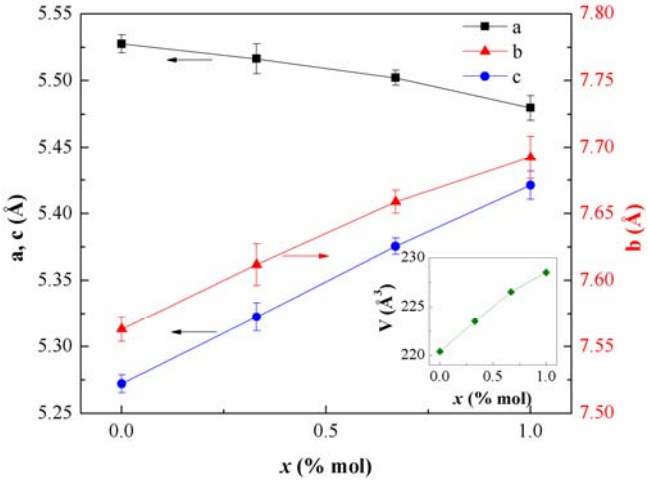

Figure 2: The lattice parameters of the *Pnma* structure of the present $Dy_{1-x}Nd_xCrO_3$ for x = 0, 0.33, 0.67, and 1 samples from the Rietveld refinements of the x-ray diffraction data. The error bars represent one standard deviation of the refined parameters from the experimental data. The inset shows the unit cell volume as a function of x. The systematic trends in the lattice parameters suggests that the successful solid-solution of $DyCrO_3$ and $NdCrO_3$ has been synthesized.

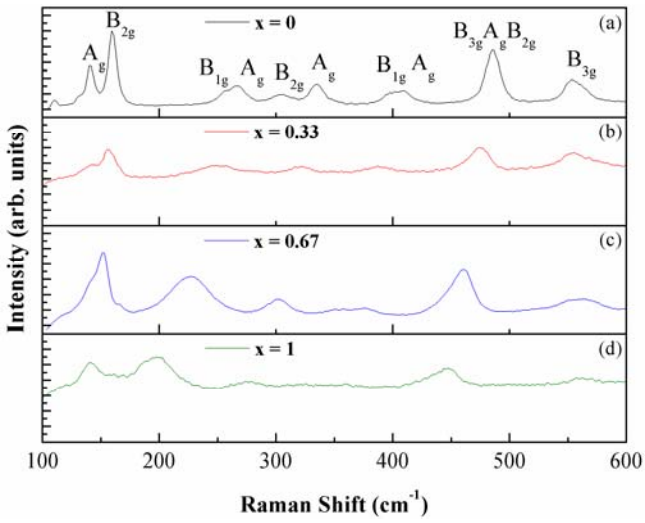

Figure 3: Room temperature Raman spectra of $Dy_{1-x}Nd_xCrO_3$ for x = 0, 0.33, 0.67, and 1 (a-d) showing the evolution of the phonon modes with Nd concentration. The systematic changes in the position of the phonon modes with x, further corroborates the incorporation of Dy into $NdCrO_3$ in the solid-solution.

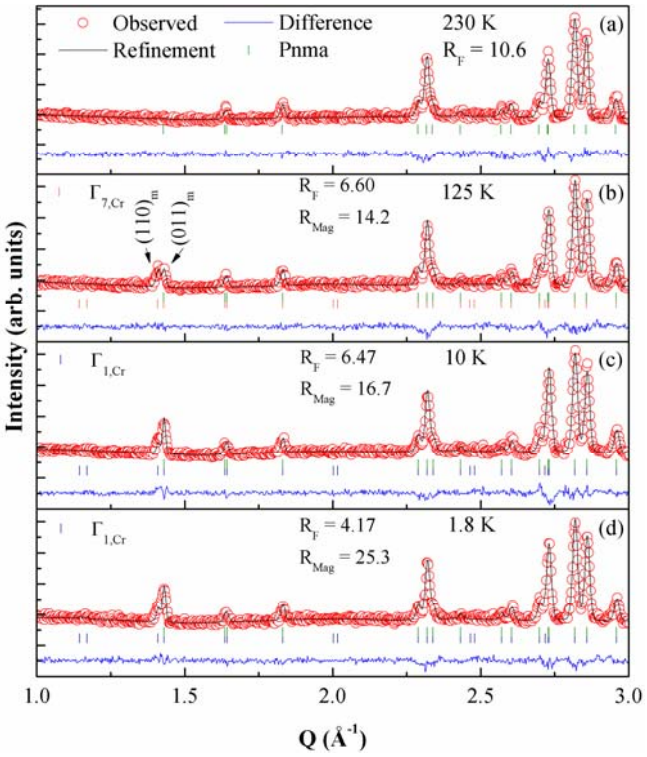

Figure 4: Neutron diffraction (red points) data, Rietveld refinement (black curve), nuclear Bragg positions (green vertical dashes), magnetic Bragg positions (orange vertical dashes for $\Gamma_{7,Cr}$, and blue vertical dashes for $\Gamma_{1,Cr}$), and difference between the refinement & the observed data (blue curve) for $Dy_{0.33}Nd_{0.67}CrO_3$ pellet at 230 K (a), 125 K (b), 10 K (c), and 1.8 K (d) under zero-field cooled conditions. The reliability factors for both the atomic structure (R_F) and magnetic structure (R_{Mag}) are also reported for each of the refinements. Note the change in the intensity of the $(110)_m$ magnetic peak at 1.409 Å, signifying the change in magnetic structure (from paramagnetic at 230 K, to Γ_7 at 125 K, to Γ_1 at 10 K and 1.8 K).

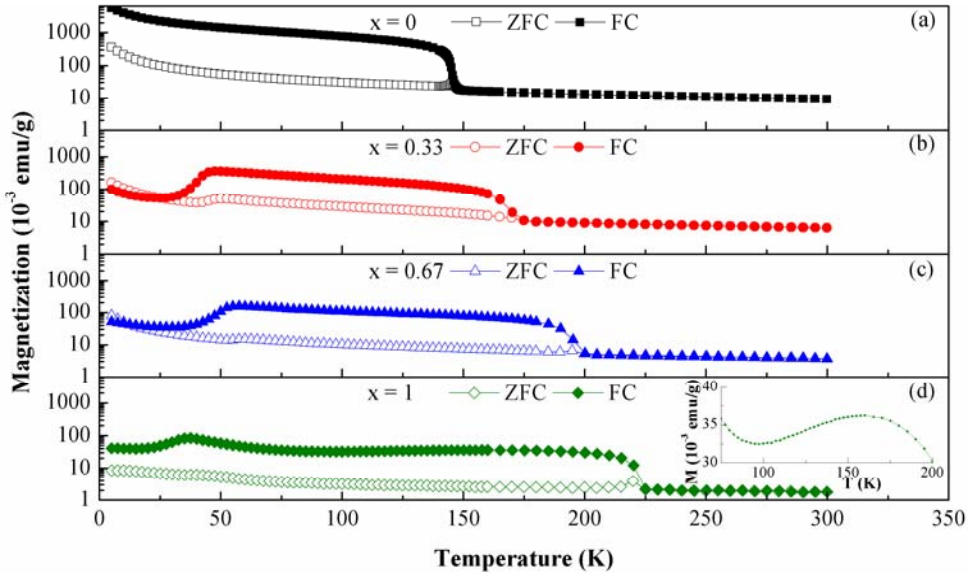

Figure 5: The temperature (T) dependence of the magnetization (M) in both zero-field cooled (ZFC) and field cooled (FC) modes for $Dy_{1-x}Nd_xCrO_3$ where x = 0 (a), 0.33 (b), 0.67 (d), and 1 (d). Note that all of the plots have identical logarithmic vertical axes. The Néel temperature (T_N) and spin-reorientation transition (T_{SR}) can be seen as changes of slope in the FC curve and peaks in the ZFC curve.

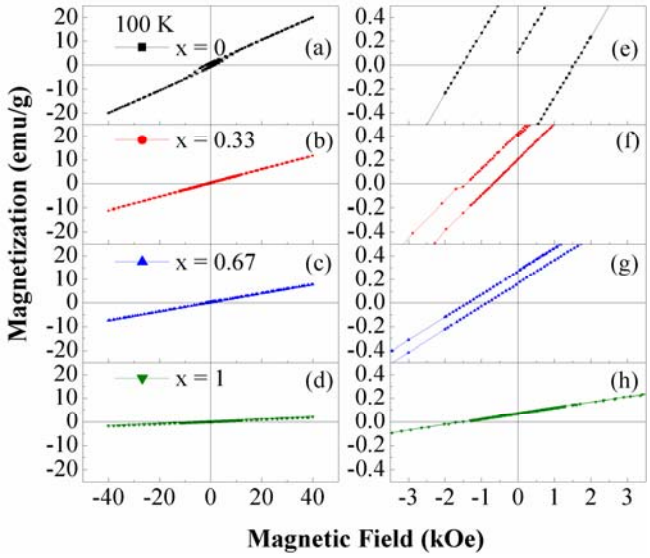

Figure 6: Isothermal magnetization measurements of $Dy_{1-x}Nd_xCrO_3$ for x = 0, 0.33, 0.67, and 1 (a-d) at 100 K. Parts (e-h) show zoomed in plot of the magnetic field near the origin from the data in (a-d), respectively. This plot clearly shows the exchange bias for x = 0.33, 0.67, and 1.

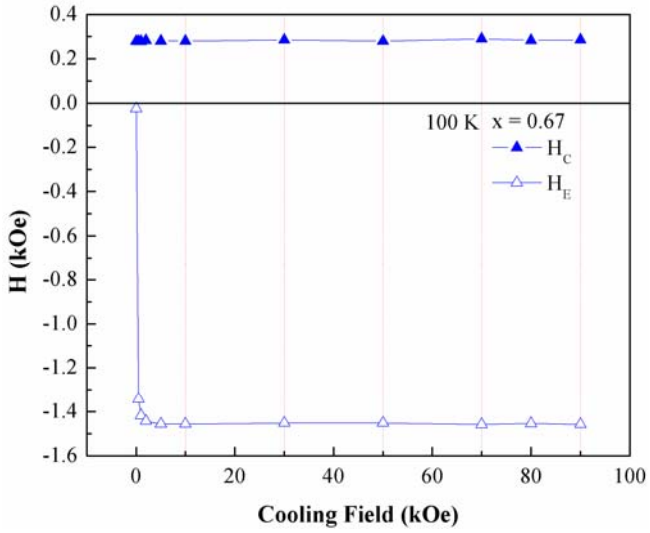

Figure 7: The dependence of coercive field (H_C, closed symbols) and exchange bias (H_E, open symbols) on the strength of the cooling field for the x = 0.67 sample at 100 K. The H_C is independent of the cooling field while the H_E saturates quickly.

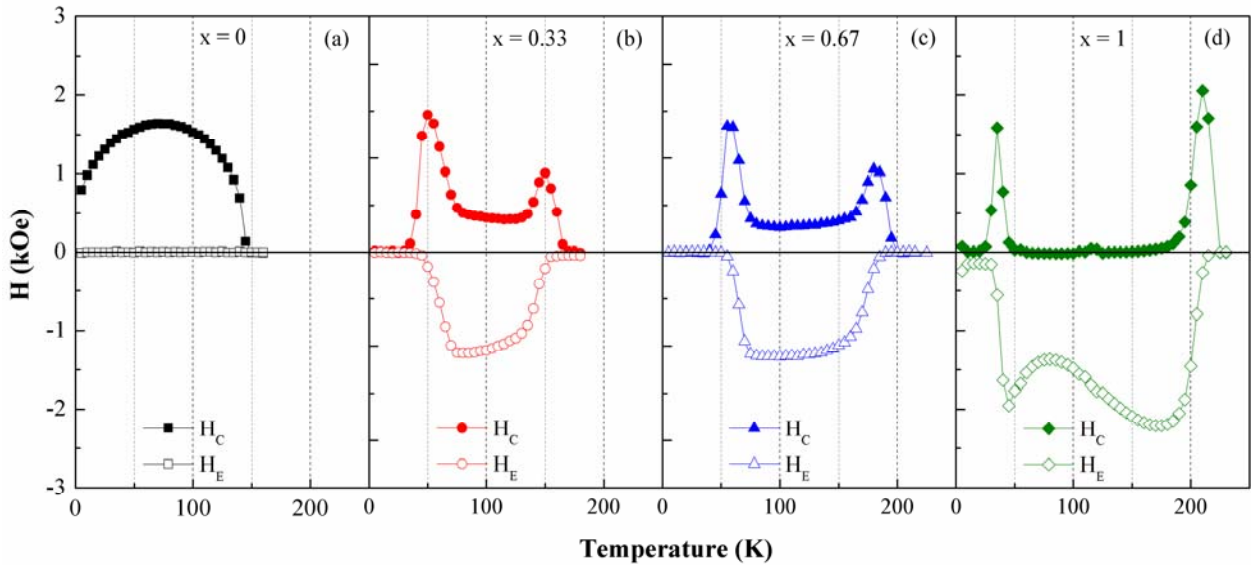

Figure 8: The temperature dependence of the coercive field (H_C, closed symbols) and exchange bias (H_E, open symbols) for $Dy_{1-x}Nd_xCrO_3$, where x = 0 (a), 0.33 (b), 0.67 (d), and 1 (d). These plots clearly show peaks in the H_C corresponding to the onset of H_E which become more pronounced with increasing x.

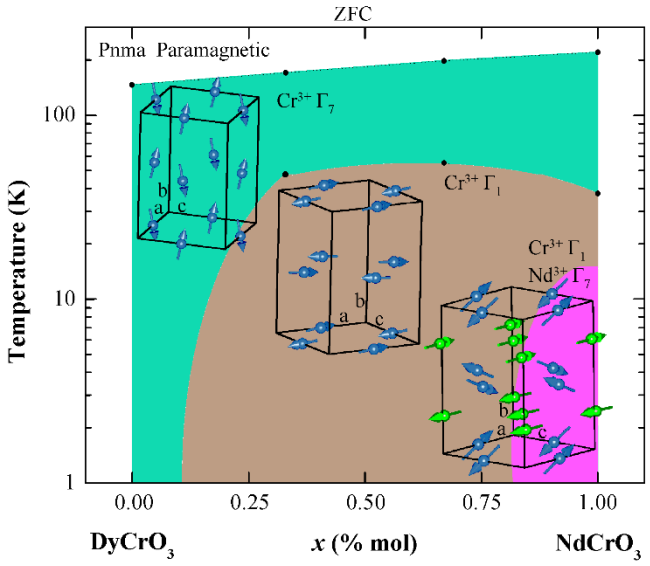

Figure 9: The zero-field cooled (ZFC) magnetic phase diagram of the $Dy_{1-x}Nd_xCrO_3$ solid-solution. The magnetic structure was determined by using the symmetry consistent irreducible representations at **k** = (0,0,0) to do the Rietveld refinements of the neutron diffraction data. The boundaries between the paramagnetic and Γ_7 region, and the Γ_7 region and the Γ_1 region were determined from bulk magnetization measurements. The region of Nd^{3+} magnetic Γ_7 order is consistent with the results of the refinement of the neutron diffraction data at 10 K and 1.6 K for $x = 1$. Representations of the magnetic structures are shown in the respective regions. The Cr^{3+} moments are shown in blue and the Nd^{3+} moments are shown in green.

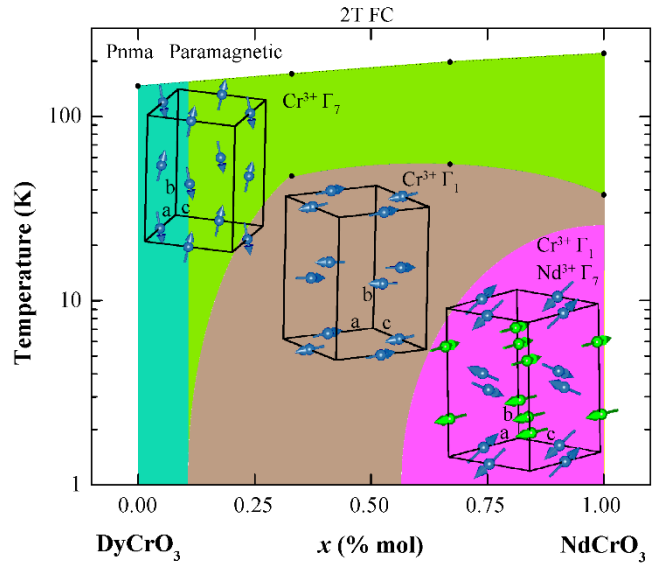

Figure 10: The proposed 2 T field cooled (FC) phase diagram of the $Dy_{1-x}Nd_xCrO_3$ solid-solution. The highlighted portion of the Cr^{3+} Γ_7 region shows where region where the exchange bias is observed. The increase in the size of the Nd^{3+} Γ_7 region is consistent with the neutron diffraction results at 10 K and 1.8 K for $x = 0.67$, and 10 K and 1.6 K for $x = 1$.